2024 IEEE International Conference on Robotics and Automation (ICRA 2024)
May 13-17, 2024. Yokohama, Japan

VWDER:A Variable Wheel-Diameter Ellipsoidal Robot

Ziao Qin,Jingzhou Song,Xinglong Gong, Changrui Liu*
School of Automation, Beijing University of Posts and Telecommunications,
No. 10, Xitucheng Road, Haidian District, Beijing, China
596908477@qq.com sjz2008 @bupt.edu.cn gongxilong@bupt.edu.cn *lcrlgmll@bupt.edu.cn*

Abstract—In recent years, many researchers have conducted extensive research on spherical robots due to their high flexibility and anti-overturning capabilities. Nevertheless, compared with legged and traditional wheeled robots, spherical robots face certain limitations. The spherical robot is composed of a closed spherical shell structure, which makes the capacity of carrying workloads weak. At the same time, the single point contact with the ground cause the contact friction force with the ground is small, so it is hard to climb obstacles such as steps and doorsill. Therefore, we propose a new solution: the variable wheel diameter ellipsoidal robot (VWDER), which combines the characteristics of two-wheel differential driven robot and spherical robot driven by equivalent pendulum.VWDER is equipped with six retractable shell-shaped legs on each side and this innovative design allows both wheels to independently change diameter while rolling. The main frame of the VWDER can keep the top of the frame facing up under the action of equivalent pendulum during the locomotion, which makes it possible to carry workloads such as manipulator arms, cameras, IMU etc. The VWDER robot can climb steps or doorsill using its two adjacent shell-shaped legs. This paper introduces the design of the VWDER and analyzes the kinematics and dynamics of the VWDER. The experimental results verified the performance of the VWDER, including its autonomous opening and closing, obstacle crossing, automatic reorientation and slope climbing etc.

Index Terms - Spherical Robot, Variable Wheel Diameter, Ellipsoidal Robot, Trafficability, Retractable Mechanism.

I. INTRODUCTION

In recent years, the working environments faced by robots have become more complex, thus placing higher demands on their performance. Currently there are three types of robots which are widely used,including legged, wheeled and spherical robots. Although legged robots have better obstacle-crossing ability, they have higher energy consumption and weaker anti-tipping ability[1]. Wheeled robots have good load capacity, but their obstacle-crossing ability is weak[2][3]. Spherical robots can swerve flexibly and have good anti-tipping ability, but they are weak in adapting to complex road conditions and are not easy to carry working loads[4]. How to balance the energy efficiency of the locomotion and the obstacle-crossing ability becomes a problem needed to solve for the mobile robot.

In this paper, a Variable Wheel Diameter Ellipsoid Robot (VWDER) is proposed (as shown in Fig.1), which has a retractable structure for enhancing the ability of striding over obstacles. The main contributions of this paper are as follows.

1) We proposed a variable diameter ellipsoidal robot VWDER that combines the advantages of legged robots, wheeled robots, and spherical robot and completed the design of the overall mechanism of the robot.

2) Autonomous reorientation, obstacle crossing and slope climbing are implemented using the Mahony complementary filtering algorithm based IMU data fusion and the PID motion control.

Fig.1. Variable wheel diameter ellipsoid robot.

II. RELATED WORK

Researchers addressed issues in traditional robots with irregular rolling and retractable mechanisms. Wenhua Chen[6] introduced a radial folding wheel for smooth movement of robot. Chun Zhang[7] developed a wheeled robot with variable diameter on the 3-RRR plane[8]. Takuma Nemoto[9] designed a caster compound rolling robot with both rolling and walking modes. Kun Xu[10] created NOROS, a hexapod wheel leg deformable robot switching between wheel rolling and leg walking. Dae young Lee[11] designed a deformable wheel robot with three motion modes. Qianqian Zhang[12] proposed a deformable two-wheel mobile mechanism for quick rolling and obstacle overcoming. These wheeled deformable robots exhibit variable wheel diameter or versatile deformations, enhancing motion performance.

In spherical robot field, Liang Lu[13] developed an active retractable shock-absorbing mechanism for a spherical scout robot. Wenchuan Jia[14] proposed a deformable robot with spherical rolling and quadruped walking capabilities adapting to terrain changes. Nathaniel Lee[15] designed a point-supported spherical robot using rounded bumpers on an icosahedron. Ryo Abe[16] proposed a spherical shell robot rolling on legs. Qiang Zhan[17] presented a deformable spherical mobile robot contracting for storage and expanding for movement. These spherical retractable robots exhibit flexible motion characteristics, enhancing their performance through deformation.

Different form the aforementioned robots, we designed a Variable Wheel Diameter Ellipsoidal Robot (VWDER), which incorporates a retractable linkage mechanism on the sphere into the two-wheel differential driven robot with equivalent pendulum. It has more compact structure and can trade off the requirements of obstacle-crossing,

maneuverability and energy efficiency of the robot locomotion.

III. SYSTEM DESCRIPTION

heel consisting of a half spherical shells. An umbrella-shaped retractable mechanism on the robot shell allows for flexible adjustments of the wheel diameter during movement, enabling obstacle-crossing.

Fig.2 illustrates the schematic diagram of the mechanism and the 3D model. Inside the robot, we use the main frame as an equivalent pendulum to replace the real pendulum, positioning the overall center of gravity directly beneath the robot body. This mechanism serves a dual purpose, providing driving torque and ensuring the robot remains stable without overturning during movement. When the equivalent pendulum is unable to provide sufficient torque in locomotion mode, auxiliary wheel can be released to assist the robot's motion.

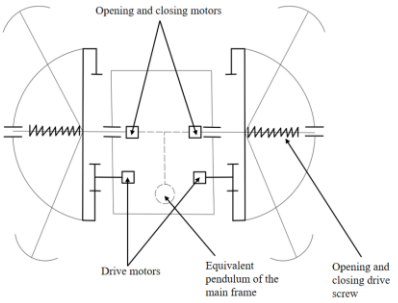

(a).schematic diagram of the robot mechanism.

(b).the 3D model of the robot.

Fig.2. schematic diagram of the robot mechanism and the 3D model

The VWDER robot features a total of twelve retractable mechanisms, evenly arranged on the surface of the spherical shell with six on each side. These mechanisms are symmetrically distributed, and each pair of six mechanisms on one side forms a V-shape with a $60°$ angle. This arrangement allows the six retractable mechanisms on each side to sequentially contact the ground, effectively forming two driving wheeled legs for obstacle crossing.

As shown in Fig.3, the two half-spherical on both sides of the robot are powered by a drive motor and an opening and closing motor that drives the retractable mechanism. The driving motor drives a pinion gear, which drives the rotation of the internal gear, thereby driving the movement of the robot. The retractable mechanism is driven by the opening and closing motor for opening and closing of the robot. The VWDER can operate the retractable mechanism simultaneously during robot motion, and they do not interfere with each other.

The gear ratio between the pinion gear of the VWDER and the large ring-gear (inner gear) is 1:6, allowing the motor

1) Robot Design

As shown in Fig.1, the VWDER robot employs a double-wheel differential movement mechanism, with each w

torque to be amplified by a factor of 6. This amplification enables the robot to perform tasks that require a large torque.

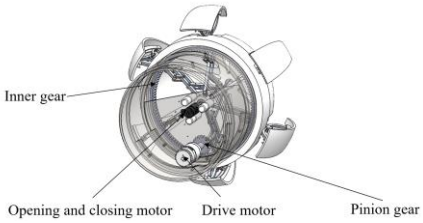

Fig.3. Semi-structural model of the robot.

The specification desired of VWDER and the achievable performance indexes of the prototype robot are shown in Table I. The robot has a mass of 15kg, with the main frame weighing 10kg. The maximum motion speed required is 1m/s, and the desired acceleration is 1m/s^2. The robot is designed to climb slopes with a maximum angle of $10°$. The maximum opening radius is 220mm, and the radius of the spherical shell is 150mm.The maximum movement speed of the VWDER experimental prototype is 1.5m/s and the robot acceleration reaches 1.2m/s^2. The maximum climbing angle is 12°, and the achieved maximum obstacle clearance height is 65mm, which meet the required index.

TABLE I

VWDER MAIN PERFORMANCE

Parameters	symbolic	value	achievable performance indexes
Robot mass	m	$15kg$	$15kg$
Main frame mass	m_{fp}	$10kg$	$10kg$
Maximum movement speed	V	$>1m/s$	$1.5m/s$
Acceleration	a	$>1m/s^2$	$1.2m/s^2$
Maximum climbing angle	δ	$>10^{\circ}$	12°
Obstacle clearance height	l	$>50mm$	$65mm$
Maximum opening radius	L	$220mm$	$220mm$
Spherical shell radius	R	$150mm$	$150mm$

2) Hardware

The architecture of the VWDER hardware is shown in Fig.4. It consists of five main modules including power supply module, upper computer, lower computer, sensor module, CAN bus center board, sensing modules, actuation modules, and extension modules.

The power supply module provides power distribution to all the aforementioned modules.Within the upper computer module, the command transmitter utilizes the SPI protocol to transmit control commands to the lower computer module. Additionally, the upper computer debugging software communicates with the lower MCU to test the control algorithms. The Sensing modules feedback information from

sensors such as IMU and sends them to the upper computer for robot planning and controlling via the CAN bus.The actuation modules receives the control commands via CAN bus and executes the tasks that the upper computer planned. This modular design allows for the seamless expansion of additional modules based on the requirements of new tasks. These expansion modules can connect to the underlying control module through CAN communication.

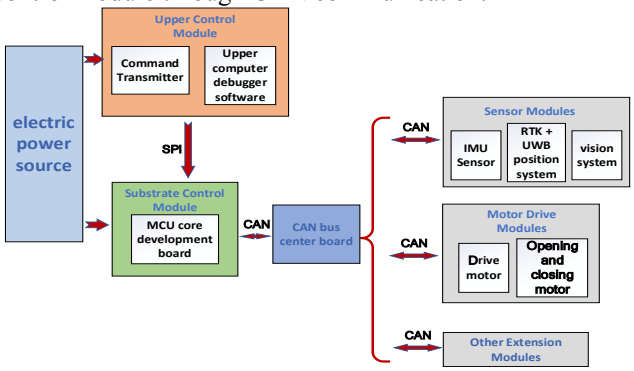

Fig.4. The architecture of the robot hardware system.

IV. THE RETRACTABLE MECHANISM DESIGN

The VWDER incorporates a highly efficient retractable mechanism that significantly enhances its obstacle-crossing maneuverability. This mechanism, shown in Fig.5(a), comprises a slider (component 1) and connecting rods (components 2-7), allowing for versatile and controllable deformation with single-motor control. The 3D model in Fig.5(b) reveals a servo motor driving a trapezoidal screw, ensuring both rapid expansion and contraction of the retractable mechanism. The self-locking function of the trapezoidal screw secures the mechanism in the expected place after expansion.

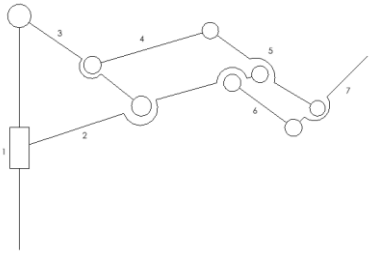

(a).Schematic diagram of single retractable mechanism

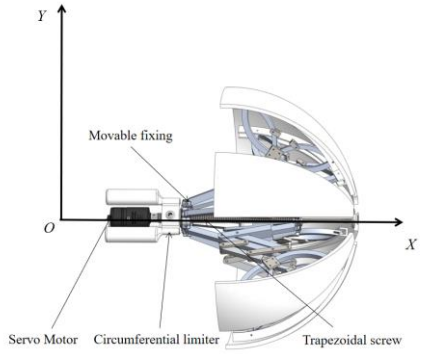

(b).3D model of retractable mechanism

Fig.5. The retractable mechanism.

In Fig.6, the movable and non-movable fixings secure the umbrella-like mechanism on the screw ends using bearings, with a shaft sleeve connecting to the spherical shell to allow the six umbrella-like legs rotating along with the spherical shell. During the retractable mechanism's opening and closing, the trapezoidal screw's rotational motion converts to axial movement of the screw nut.

The screw nut circumferential limiter, depicted in Fig.6, connects with the screw nut by a bolt, enabling it move axially along with the screw nut. In the circumferential direction, the movable fixing mounts onto a bearing with a end cap, and then they are setup onto the screw nut. This design allows the movable fixing to rotate around the center axis of the trapezoidal screw and make the opening and closing of the retractable mechanism interference-free with the spherical shell's rotation, which facilitate the mechanism real-time deformation with the locomotion of the robot.

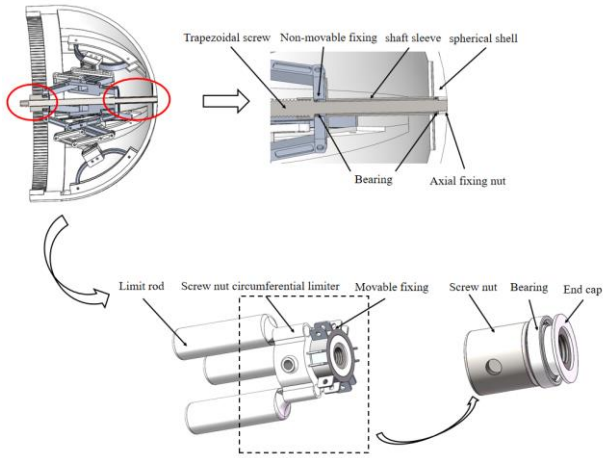

Fig.6. Retractable Mechanism Connection with Spherical Shell

V. KINEMATICS AND DYNAMICS ANALYSIS

1) Retractable Mechanism Kinematics Analysis

As shown in Fig.7, the motion of the multiple linkages in the retractable mechanism ultimately affects the position of point I. By establishing a kinematic model of point I, the position of the retractable mechanism at place can be determined. Figure 7 shows the linkages kinematic relationship in the X-axis and Y-axis direction.

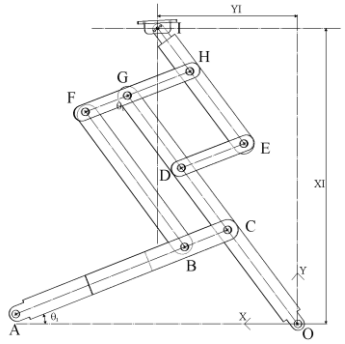

Fig.7. Linkages kinematic relationship in the X-axis and Y-axis direction

$$Y_I = \left[\left(1+\frac{l_{CD}+l_{EI}}{l_{OC}}\right)l_{AC}+l_{DG}\right]\sin\theta_1 \tag{1}$$

$$l_{OA} = l'_{OA} + v_A \Delta t \tag{2}$$

$$\begin{cases} X_I = \dfrac{l_{OC}+l_{CD}+l_{EI}}{l_{OC}}(l_{OA}-l_{AB}\cos\theta_1)-l_{DG}\cos\theta_1 \\ l_{OA}^2+l_{AC}^2-2l_{OA}l_{AC}\cos\theta_1 = l_{OC}^2 \end{cases} \quad (3)$$

The equation 1-3 give the kinematic relation between the point I and the travelling speed v_A of the screw nut. Where $l_{OA}^{'}$ is the length of OA when the linkages mechanism fully closes, which varies with the variation of the distance between two points in OA along the X-axis. The $X_I$and the Y_I respectively represent the distance from point I on the linkage mechanism to the X-axis and Y-axis, which can be expressed by the length of the linkage. The l_{ij} denotes the the lengths of the corresponding rods, which are constants.

2) Dynamics Analysis

a) Starting acceleration

When the VWDER starts moving from rest on the ground, it encounters resistances such as rolling friction resistance, slope resistance, and air resistance. Since the robot run at a relatively low speeds, the impact of air resistance can be negligible. Assuming no slip between the wheel and the ground, the maximum acceleration of the robot can be calculated using the following equation.

$$ma = 2F^* - F_R - F_{St} \quad (4)$$

Where a is the starting acceleration, $F^*$is the maximal driving force of the robot, F_R is the rolling friction resistance and F_{st} is the slope resistance.

When in contact with the ground, the VWDER experiences rolling friction with the coefficient $f_R(f_R = 0.2)$. The rolling friction resistance on a sloped road α_{St} is then expressed.

$$F_R = f_R mg\cos\alpha_{St} \quad (5)$$

When the robot rolls on a slope, the component of the gravitational force parallel to the surface creates slope resistance F_{St}, impeding the startup. The slope resistance is determined by the slope angle α_{St} as follow.

$$F_{St} = mg\sin\alpha_{St} \quad (6)$$

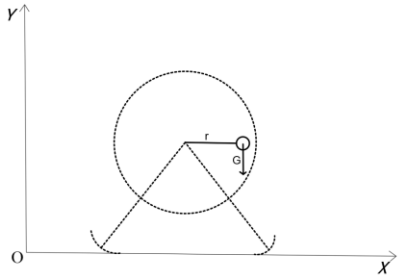

Fig.8. Schematic of the maximum swinging height of the equivalent pendulum.

equivalent pendulum mass: $m_{Hp} = 10$kg, force arm: $r = 90$mm.

Fig.8 shows the maximum swinging height of the equivalent pendulum at robot starting. The mass of the robot is 15kg, taking certain margin here with $m = 20$kg. The equivalent pendulum can supply a maximum counter-torque of $T^*(T^* = m_{Hp}r = 9\text{N}\cdot\text{m})$, where the m_{Hp} is the equivalent pendulum mass. By substituting $T^*(T^* = 9\text{N}\cdot\text{m})$ and $R(R = 0.12\text{m})$ into $F = T^*/R$, where R is the equivalent pendulum reference radius, F^* can be obtained as 75N. These values can be substitute into formula (4), then we can get the maximal starting acceleration $a_{max} = 1.55\text{m/s}^2$ when α_{St} is 0.

It is noted that the VWDER incorporates a single auxiliary wheel, which is connected to the middle frame, so that it can provide more strong counter-torque when the robot need to cross the big obstacles. The auxiliary wheel would be retracted when the robot moves on a flat ground.

b) Step climbing dynamics analysis

The step-climbing is pivotal for evaluating the robot obstacle crossing capabilities. Here we deduce the condition that the VWDER can climb a step. As shown in Fig.9, the equivalent pendulum provides the needed counter-torque when the robot climbs the step. The position represented in the dotted line means that the robot climbed up the step. Thus, the necessary conditions of step-climbing can be determined by evaluating whether the initial moment meets the following equation.

$$m_{Hp}gr = G(L\sin\theta - r) \quad (7)$$

Where the gravity of the equivalent pendulum is G. The distance from the gravity center point D of the middle frame to the rotation center C is force arm r ($r = 90$mm). The maximum opening radius of the robot shell is L ($L = 220$mm). The above parameters substituting into equation (7) yields $\theta = \frac{5\pi}{21}$. Based on the trigonometric relation, the step height that the VWDER can climb up can be obtained as following.

$$H = L\cos(\frac{\pi}{3} - \theta) - L\cos\theta \quad (8)$$

By calculation, $H = 51mm$. Therefore, it is possible to cross steps smaller than 51mm.

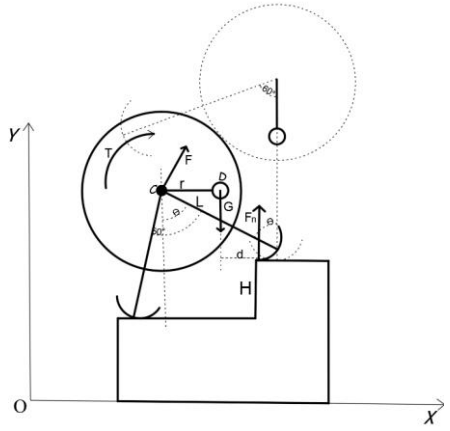

Fig.9. Diagram of robot step climbing motion

VI. CONTROL ALGORITHM ANALYSIS

For a robot, the capability to sense and control its position and orientation during motion is of paramount importance. The logic diagram for attitude control of the VWDER is depicted in Fig.10. The VWDER employs a 9-axis IMU to obtain the attitude data of the robot, where encompassing a 3-axis gyroscope, a 3-axis accelerometer, and a 3-axis magnetometer. The robot can acquire real-time position and orientation data feedback from IMU to plan and control its movements and adjust the robot attitude in its locomotion.

The VWDER uses the Mahony complementary filtering algorithm[18][19][20] to process the data from 9-axis IMU. The gyroscope has excellent dynamic response in high-frequency ranges but accumulates integration errors. Accelerometers, with favorable low-frequency characteristics, correct pitch and roll angle data from the gyroscope. The three-axis gyroscope measures angular velocity, with quaternions deriving the theoretical gravity acceleration direction. Simultaneously, the accelerometer measures actual gravity acceleration. Cross-multiplying these vectors of data compensates for errors.

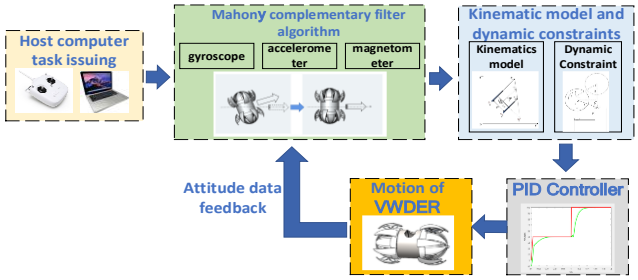

Fig.10. Attitude Control Logic Diagram

In six-axis data fusion, correcting yaw angle data using only theoretical and actual gravity vectors is challenging. The magnetometer, merging low-frequency characteristics with the gyroscope's high-frequency ones, compensates for yaw angle data.

Fig.11 illustrates the Mahony algorithm. The robot uses last moment's attitude data to predict the next moment's attitude measurement and gravity/magnetic force direction. The magnetometer's next moment vector is cross-multiplied with the accelerometer's vector, then them are outputted into the PI compensator for gyroscope correction, ultimately correcting the next moment's attitude.

The error correction method of Mahony data fusion is shown in equation (9), where ρ represents the error value, which is the sum of magnetic field deviation and gravitational acceleration direction deviation. $\overline{v}$ and v represent the actual gravitational acceleration vector and the theoretical gravitational acceleration vector, and $\overline{m}$, $\hat{m}$ denote the actual magnetic field vector and the theoretical magnetic field vector, and θ_1 and θ_2 indicate the angle between the actual vector and the theoretical vector respectively. After obtaining the vector deviation, a PI compensator can be constructed to integrate the low-frequency information of the accelerometer and magnetometer and complement it with the gyroscope, where the PI compensator is used as a low-pass filter.

$$|\rho| = |\overline{v}| \cdot |\hat{v}| \cdot \sin\theta_1 + |\overline{m}| \cdot |\hat{m}| \cdot \sin\theta_2 \quad (9)$$

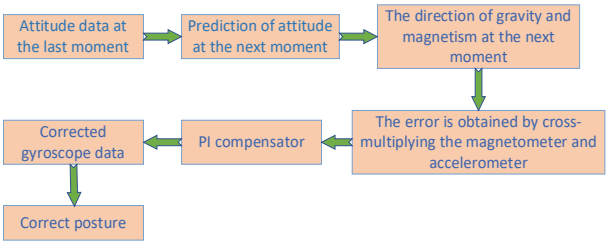

Fig.11. The flow chart of Mahony complementary filtering algorithm

Fig.12 illustrates the robot's attitude control using a three-layer PID structure. The upper computer inputs the desired attitude, corrects gyroscope data with an outer PI compensator, obtains desired speed through kinematic modeling, and tracks velocity via a second-layer speed loop PID. The output is sent to the electrical controller through the CAN bus. Precise motor speed control is then achieved through the controller's internal current loop PID, completing attitude adjustment.

During operation, motor encoder feedback provides real-time motor speed information, enabling closed-loop control. PID adjustments based on the deviation between real-time feedback and set values ensure precise linear and angular speed control. Simultaneously, 9-axis IMU feedback enables closed-loop control of pose. In cases of deviation from the expected path due to external interference, Euler angle differences trigger PID control for rapid readjustment of the robot's motion posture.

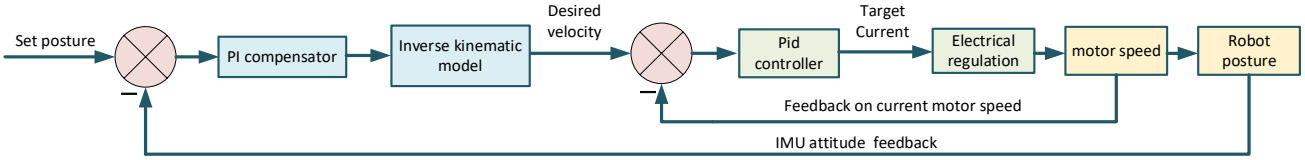

Fig.12. VWDER control flowchart

VII. Experiments and Results

1) Robot opening and closing experiment

We conducted experiments involving the robot one-side and two-side opening motions. When one side of the half-spherical shell can not contact with the ground, the retractable mechanism can extend itself to keep the robot horizontal and roll on the ground steadily, displaying its terrain adaptability. When the robot both sides opening, it can execute regular locomotion and successfully overcome the obstacles. Its maximum stretching distance can reach 70mm as shown in Fig.13.

Fig.13. The maximum stretching distance

2) Robot obstacle crossing experiment

a) Plastic foam board obstacle crossing

We compared the obstacle-crossing of the VWDER under retractable mechanism opening state with its closing state. As show in Fig.14, when the robot faces a white plastic foam board on the lawn, it fails to climb it in the shell closing state but smoothly ascends the 5cm height foam board in the shell opening state. It can also swiftly transfer state from the opening to the closing after overcoming the obstacle.

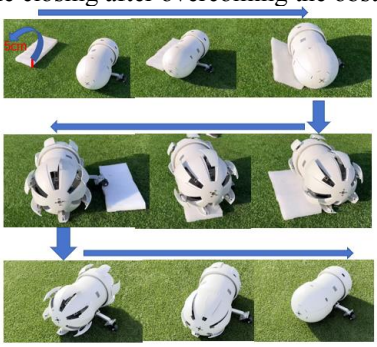

Fig.14. Robot obstacle surmounting experiment.

b) Doorsill obstacle crossing

For special tasks like indoor hazard detection, a robot may face challenges such as high barriers that conventional spherical robot or wheeled robot can't overcome. The VWDER using its adaptable wheeled legs can easily cross the obstacles like doorsill. Having crossed the doorsill, it can speedily transform into a two-wheel model for energy efficient locomotion via closing the retractable mechanism. As shown in Fig.15, the robot successfully surmounted a 5cm height doorsill in a room.

Fig.15. Doorsill surmounting experiment.

c) Continuous step climbing

The VWDER has unique advantages when facing complex environments. Compared to traditional wheeled or spherical robots, VWDER can cope with continuous step obstacles. By opening the retractable mechanism and stretching out the auxiliary wheel, the VWDER successfully climbed up the steps, (with each step height of 6.5cm), as shown in Fig.16. This experiment demonstrates the ability of VWDER in dealing with complex environments.

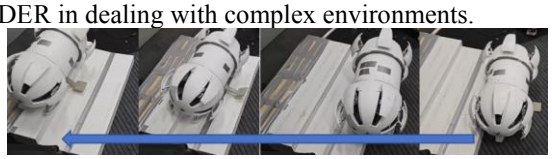

Fig.16. Continuous step climbing experiment.

3) VWDER locomotion performance experiment

We tested the locomotion performance of VWDER with and without auxiliary wheels on standard plastic tracks. As shown in Fig.17. When carrying an auxiliary wheel, its maximum speed is $1.54m/s$. When not carrying auxiliary wheels, its maximum speed is $1.53m/s$, which meet the design requirements for speeds greater than $1m/s$.

In the acceleration testing, the robot accelerated from $0m/s$ to $1.55m/s$ within 1.20 seconds when carrying an auxiliary wheel, and within 1.30 seconds when without the auxiliary wheel. The average maximum acceleration is $1.29m/s^2$ (With auxiliary wheel) and $1.19m/s^2$ (Without auxiliary wheel) respectively, which both meet the requirements of $1m/s^2$.

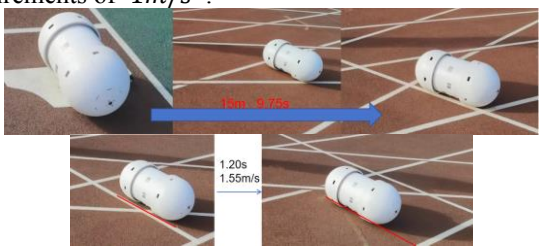

(a).With auxiliary wheel

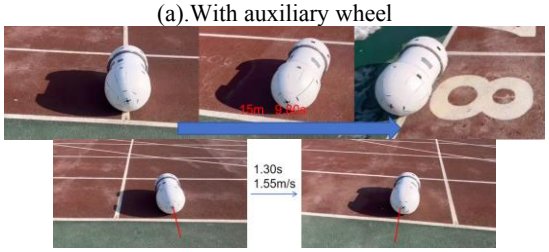

(b).Without auxiliary wheel

Fig.17.Maximum velocity and acceleration testing

4) automatic reorientation

When the robot is moving under complex road conditions, it is inevitable that the robot will deviate from course due to external disturbance force caused by uneven road surface. Therefore, we have designed the automatic orientation-adjusting function, so that the robot can quickly return to the planned direction and travel normally.

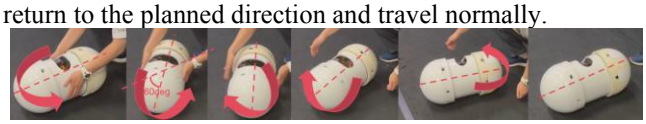

Fig.18. Robot automatic aligning experiment.

As shown in Fig.18, the robot is forced to change the orientation, causing it deviate the set direction by 60°. The robot always can correct its orientation according to the data feedback from IMU and adjust itself to the set direction. The adjust time is 0.5s, and the angular velocity of aligning can reach $20rpm$.

VIII. Conclusion

In this paper, a variable diameter ellipsoidal robot VWDER is designed. The robot moves on the horizontal ground by the way of differential speed on both sides, and the wheel diameter of the robot is changed by the umbrella type retractable mechanism.The robot has the advantages of anti-overturn and terrain adaptability. The VWDER robot can adjust its orientation according to the data feedback from IMU and can cross doorsill and steps etc. obstacles, climb up slope. The VWDER can be applied to hazard detection and safety inspection etc. fields. In the future, we will carry manipulator on the middle frame of the VWDER to carry out different tasks and study the coupling control method of the mobile manipulator.

Acknowledgment

This work was supported by National Natural Science Foundation of China Item No. 62373063.

REFERENCES

[1] Biswal P, Mohanty P K. Development of quadruped walking robots: A review[J]. Ain Shams Engineering Journal, 2021, 12(2): 2017-2031.

[2] Michaud F, Laplante J F, Larouche H, et al. Autonomous spherical mobile robot for child-development studies[J]. IEEE Transactions on Systems, Man, and Cybernetics-Part A: Systems and Humans, 2005, 35(4): 471-480.

[3] Leong J S L, Teo K T K, Yoong H P. Four Wheeled Mobile Robots: A Review[C]//2022 IEEE International Conference on Artificial Intelligence in Engineering and Technology (IICAIET). IEEE, 2022: 1-6.

[4] Jung C, Chung W. Accurate calibration of two wheel differential mobile robots by using experimental heading errors[C]//2012 IEEE International Conference on Robotics and Automation. IEEE, 2012: 4533-4538.

[5] Yevsieiev V, Shmatko S. Analysis of Crawler Robots[D]. International Science Group, 2022.

[6] Chen W, Wu Q, Hu M, et al. Design & analysis for the configuration of a radially foldable wheel[C]//2010 IEEE International Conference on Mechatronics and Automation. IEEE, 2010: 83-87.

[7] Zhang Chun. Configuration design and motion performance analysis of a new wheel spoke rolling robot[D]. Yanshan University, 2021.

[8] Wu J, Wang J, You Z. A comparison study on the dynamics of planar 3-DOF 4-RRR, 3-RRR and 2-RRR parallel manipulators[J]. Robotics and computer-integrated manufacturing, 2011, 27(1): 150-156.

[9] Nemoto T, Mohan R E, Iwase M. Rolling locomotion control of a biologically inspired quadruped robot based on energy compensation[J]. Journal of Robotics, 2015, 2015: 7-7.

[10] Xu K, Ding X. Typical gait analysis of a six-legged robot in the context of metamorphic mechanism theory[J]. Chinese Journal of Mechanical Engineering, 2013, 26(4): 771-783.

[11] Lee D Y, Koh J S, Kim J S, et al. Deformable-wheel robot based on soft material[J]. International journal of precision engineering and manufacturing, 2013, 14: 1439-1445

[12] Zhang Q, Li Y, Yao Y A, et al. Design and locomotivity analysis of a novel deformable two-wheel-like mobile mechanism[J]. Industrial Robot: the international journal of robotics research and application, 2020, 47(3): 369-380.

[13] Lu L, Chu M. Shock Absorber Design and Analysis of a Catapult-Spherical Reconnaissance Robot[J].Advanced Materials Research,2013,662:694697.DOI:10.4028/www.scientific.net/AMR.662.694.

[14] Jia W, Huang Z, Sun Y, et al. Toward a novel deformable robot mechanism to transition between spherical rolling and quadruped walking[C]//2017 IEEE International Conference on Robotics and Biomimetics (ROBIO). IEEE, 2017: 1539-1544.

[15] Lee N J. Design of a Deformable Spherical Robot[D]. Massachusetts Institute of Technology, 2022.

[16] Abe R, Kanamori C. Development of a Spherical Shell Robot with Rolling and Legged Locomotion[J]. Journal of Robotics and Mechatronics, 2023, 35(2): 483-491.

[17] Zhan Q, Liu Z N. A deformable spherical mobile robot[J]. Applied Mechanics and Materials, 2014, 590: 422-426.

[18] Zhu Y, Liu J, Yu R, et al. Attitude solving algorithm and FPGA implementation of four-rotor UAV based on improved mahony complementary filter[J]. Sensors, 2022, 22(17): 6411.

[19] Ludwig S A, Burnham K D. Comparison of Euler estimate using extended Kalman filter, Madgwick and Mahony on quadcopter flight data[C]//2018 International Conference on Unmanned Aircraft Systems (ICUAS). IEEE, 2018: 1236-1241.

[20] Guo X, Sun Y, Wang Q, et al. Attitude measurement of permanent magnet spherical motors based on adaptive mahony complementary filtering[J]. Measurement, 2023, 222: 113608.